applied sciences

MDPI

Article

Preliminary Study on the Damping Effect of a Lateral Damping Buffer under a Debris Flow Load

Zheng Lu [1,2], Yuling Yang [2], Xilin Lu [1,2] and Chengqing Liu [3,*]

1 State Key Laboratory of Disaster Reduction in Civil Engineering, Tongji University, Shanghai 200092, China; luzheng111@tongji.edu.cn (Z.L.); lxlst@tongji.edu.cn (X.L.)
2 Research Institute of Structural Engineering and Disaster Reduction, Tongji University, Shanghai 200092, China; yangyl_tj@163.com
3 School of civil engineering, Southwest JiaoTong University, Chengdu 610031, China
* Correspondence: lcqtj@163.com; Tel.: +86-21-6598-6186

Academic Editors: Gangbing Song, Steve C.S. Cai and Hong-Nan Li
Received: 29 December 2016; Accepted: 13 February 2017; Published: 20 February 2017

Abstract: Simulating the impact of debris flows on structures and exploring the feasibility of applying energy dissipation devices or shock isolators to reduce the damage caused by debris flows can make great contribution to the design of disaster prevention structures. In this paper, we propose a new type of device, a lateral damping buffer, to reduce the vulnerability of building structures to debris flows. This lateral damping buffer has two mechanisms of damage mitigation: when debris flows impact on a building, it acts as a buffer, and when the structure vibrates due to the impact, it acts as a shock absorber, which can reduce the maximum acceleration response and subsequent vibration respectively. To study the effectiveness of such a lateral damping buffer, an impact test is conducted, which mainly involves a lateral damping buffer attached to a two-degree-of-freedom structure under a simulated debris flow load. To enable the numerical study, the equation of motion of the structure along with the lateral damping buffer is derived. A subsequent parametric study is performed to optimize the lateral damping buffer. Finally, a practical design procedure is also provided.

Keywords: debris flow; shock absorbers; buffer; impact test; numerical simulation; parametric study

1. Introduction

Debris flows can cause serious damage to infrastructures and threaten lives. There have been a considerable number of debris flows involving the destruction of mountain villages and small towns, such as the disasters which occurred in Venezuela in December 1999 [1] and in Zhouqu, China, in August 2010 [2]. Mountainous areas with low vegetation cover and up-and-down landform are extremely vulnerable to debris flows. Therefore, buildings in these mountainous areas are prone to damage by debris flows. Actually, buildings play an important role in resisting debris flows. Hence, drastic measures are urgent to ensure buildings withstand such kinds of disasters.

Studies on buildings against debris flows specifically are relatively deficient; however, there is still some research involving mitigation measures to reduce the damage by debris flows and the interaction between debris flows and buildings [3,4]. Debris flow mitigation measures can be categorized into two classifications, namely engineering measures and non-engineering measures [5]. Meanwhile, engineering measures include drainage systems [6,7], check dams [8–10], and flexible barriers [11], etc., while non-engineering measures involve disaster warning and evacuation systems, retrofitting and reinforcement of buildings [12], etc. In this paper, the main goal is to propose some specific structural measures to reduce the damage to buildings caused by debris flows from the perspective of building retrofitting.

It is known that debris flow is characterized by high velocity, strong striking force and severe destruction [13]. Therefore, if prevention measures are based on reinforcement, the construction cost would be drastically high, while the safety of buildings still cannot be guaranteed for the randomness of debris flows. Therefore, people should seek a method to retrofit buildings with some devices or equipment of a lower cost. On the other hand, the application of structural vibration control in aseismic engineering field provides a new solution to this problem. In civil engineering, the systematic knowledge of structural vibration control was first introduced by Yao [14], and structural control plays an important role in engineering nowadays [15–17]. It is a typical method to attach devices [18] or to study the failure modes [19] to prevent structures from being destroyed under earthquake. Moreover, in the field of vehicle control, the semi-active suspension [20–23] and active suspension [24] play an important role in guaranteeing both safety and comfort of cars. In this way, devices or equipment suitable for different structures or applicable to different scenarios (e.g., [25–30]) are put forward to reduce the structure's response under different dynamic loads.

Enlightened by various structural control methods [25–30] and semi-active suspensions [20–23] as well as active suspensions [24], a lateral damping buffer is proposed to retrofit buildings in debris flow-prone areas. Specifically, it is a combination of traditional buffer and shock absorber. By attaching such devices to existing buildings, the structures' debris flow resistance can be enhanced a lot, especially when the loading level is high; the maximum acceleration response can be reduced by nearly half. In addition, the construction is fairly simple because the buffer can be directly attached to the existing structure without large-scale reconstruction. To examine the performance of the lateral damping buffer, an impact test of such a device attached to a two-degree-of-freedom (DOF) structure under a simulated debris flow load is completed. In China, there are mainly three types of domestic structures in mountain regions of the western area, namely, reinforced framed structures, masonry structures, and reinforced masonry structures [31]. In this paper, we take a frame structure as an example to study the effect of the buffer. Then, a numerical simulation is performed to validate its rationality. Finally, based on parametric study, a practical design procedure is provided.

2. Schematic of a Lateral Damping Buffer

A schematic of the lateral damping buffer is shown in Figure 1. Two pieces of board are connected by springs, acting together as a cushion to the impact. In addition, eight boxes with eight particles uniformly adhere to one of the boards, whose main function is to enlarge the damping as energy-dissipating dampers. Meanwhile, the diameter of the particles is 12 mm, and each particle weighs 7 g. The size of the boxes is 25 mm × 25 mm × 18 mm, and each one weighs 6 g.

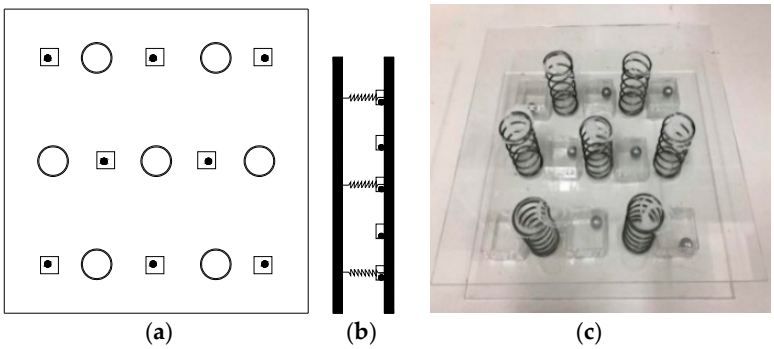

Figure 1. A lateral damping buffer: (**a**) Front view; (**b**) Side view; (**c**) Model picture.

As mentioned above, a lateral damping buffer takes effective roles in two ways. Firstly, it is installed in the impact point, and works as a cushion. In this way, the lateral damping buffer can reduce the peak intensity of applied stresses effectively at the beginning of impact. Then, the particles collide with the boxes to enlarge the damping coefficient of the system, so that the subsequent vibration

of structures can be further reduced. On the whole, the lateral damping buffer reduces the response of structures subjected to debris flow impacts by decreasing both the peak value and the mean value.

3. Experiment Validation

3.1. Experiment Design

In the experiment, responses of an uncontrolled structure and a structure with the lateral damping buffer under simulated debris flows are measured to make a detailed comparison. For the buffer case, the lateral damping buffer is installed at the potential impact point, as is shown in Figure 2. In this way, the effectiveness of the lateral damping buffer can be examined. In most mountainous areas of China, the buildings to be hit are typically reinforced framed structures, masonry structures or reinforced masonry structures. In this paper, a two-degree-of-freedom frame structure is used as a primary structure, whose mass is 0.9 kg, with added mass weighing 6 kg evenly placed on the two layers. The first and second order frequencies of the structure are 3.56 Hz and 14.07 Hz, and its damping ratio is 4.0% [32].

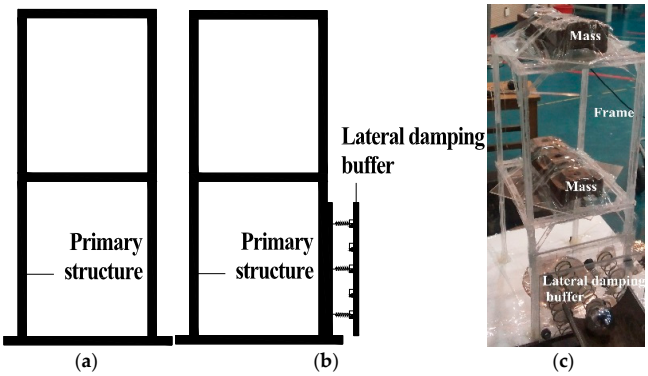

Figure 2. Schematic diagram of the test: (**a**) Uncontrolled structure; (**b**) Structure with the lateral damping buffer; (**c**) Experimental model picture.

A test site is designed according to the situation when debris flows break through and the test operability, shown in Figure 3. The loading device includes a slope with an angle of 30° on the horizontal plane and a fixed mount. Referring to other experts' experience, the load of debris flows is simulated by an impact force caused by a ball rolling down from a slope [33–35]. There is one accelerometer placed at the top of the test model to record the structural response.

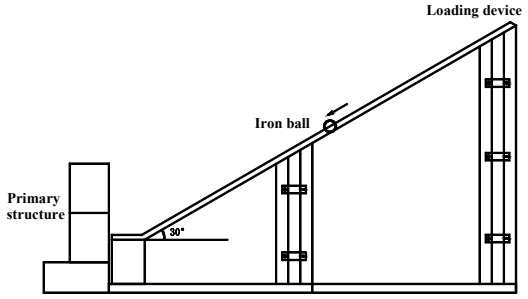

Figure 3. Experimental device.

In the test, the impact load is exerted on the primary structure when the steel ball weighing 0.51 kg rolls down from different heights. The loading procedures are divided into ten grades. The relative height of the first loading is 0.05 m, and the height difference between two loading grades is 0.05 m. Response of the structure is measured by accelerometers.

3.2. Responses in Time Domain

Figure 4 shows a typical acceleration time history curve of the structure with and without a buffer. It can be found that the response of the structure with the lateral damping buffer is smaller than that of the uncontrolled structure, in which the peak value of the acceleration is reduced evidently. The maximal acceleration response appears at the beginning of the time history curves. As is mentioned above, the lateral damping buffer can be regarded as a combination of a shock absorber and a buffer. Given that energy dissipation devices need time to work, when the maximum value of acceleration response appears, the shock absorbers in the device have not functioned yet. Therefore, the buffer of the device makes a major contribution to the reduction of the maximal acceleration response of the primary structure.

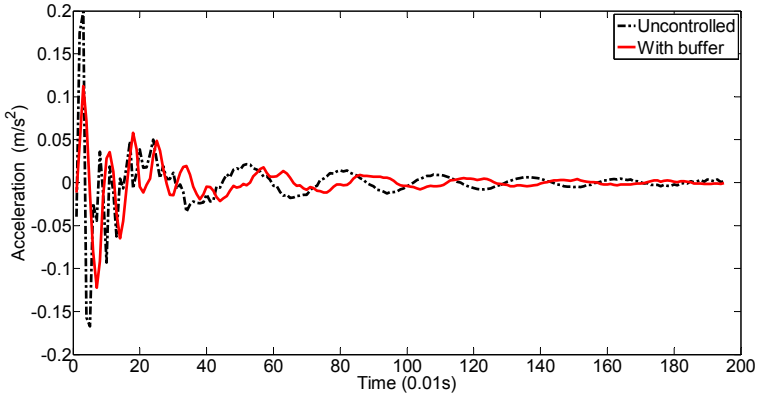

Figure 4. Time history curves of structure with/without a lateral damping buffer (grade 7).

To study the effectiveness of the damping buffer in reducing the subsequent vibration of the primary structure after impact, root mean square (r.m.s) response is taken as a measurement index. Furthermore, the influence of the buffer can be eliminated by removing the wavelengths where the peak value was.

The response reduction effects of both the maximum acceleration and the root mean square acceleration are shown in Figure 5. It can be seen that the responses of both the maximum acceleration and the root mean square acceleration of the structure with the lateral damping buffer are reduced largely. In addition, the response reduction effect is relatively small when the loading grade is low, while the response reduction effects of both the maximum acceleration and the root mean square acceleration increase step by step as the loading grade increases. That is, the larger the impact force, the better the effectiveness of the device, which is obviously beneficial to the practical engineering application.

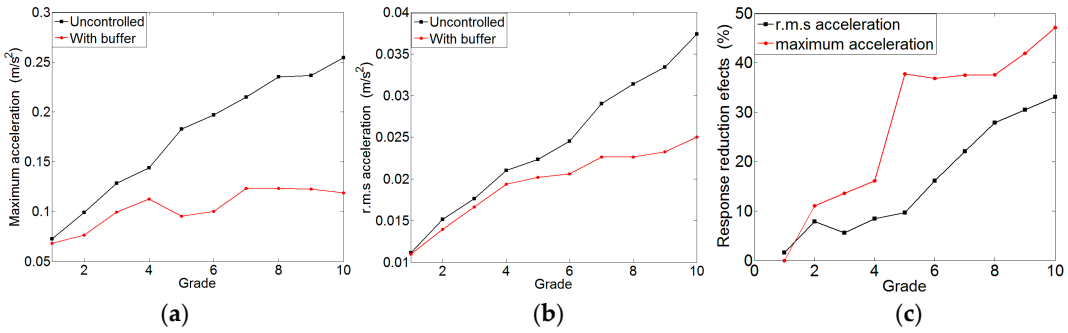

Figure 5. Acceleration response and the reduction efficiency: (**a**) Maximum acceleration; (**b**) Root mean square (r.m.s) acceleration; (**c**) Response reduction effects.

3.3. Responses in Frequency Domain

Figure 6 shows the responses of the uncontrolled structure and the structure with buffer in the frequency domain under the loading cases of grade 4 and grade 6.

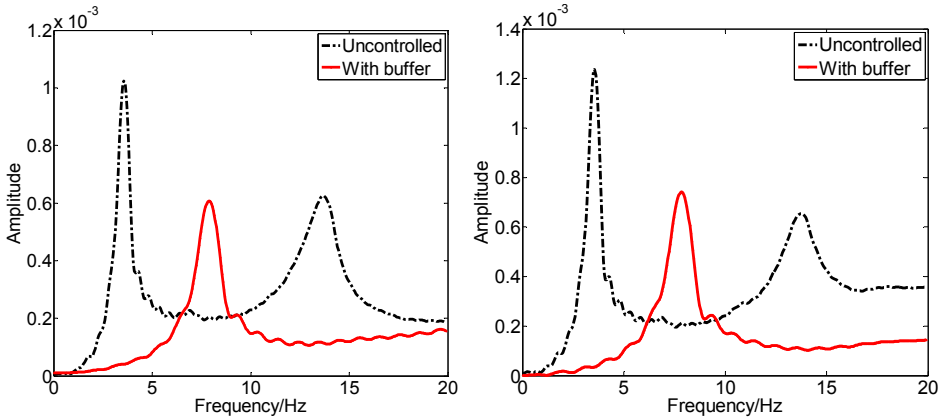

Figure 6. The frequency domain response: (**a**) Grade 4; (**b**) Grade 6.

From the figure, it can be seen that:

(1) The Fourier spectrum of the acceleration time history curve of the uncontrolled structure has two obvious peak values in the vicinity of 3.6 Hz and 14 Hz respectively, which correspond to the measured natural frequencies. However, the Fourier spectrum of the structure with buffer has just one peak value in the vicinity of 8 Hz, since the attachment of the buffer has strengthened the integrity of the structure.

(2) As for the amplitude, the response of the structure with a buffer is clearly reduced. That is, the vibration of the structure is under control and the lateral damping buffer has good effects.

(3) The Fourier spectral lines show the distribution of the vibration power of the primary structure in the frequency domain. The area under the Fourier spectral line of the structure with the buffer is smaller than that of the uncontrolled one, which shows the lateral damping buffer can greatly decrease the vibration energy of structures.

(4) Compared the response under fourth loading grade and sixth loading grade, the latter is evidently smaller than the former, indicating that with increasing impact, the buffering and vibration controlling effects of the device will increase.

3.4. Equivalent Damping Ratio

According to the test, the equivalent damping ratios are calculated based on its definition [32] (shown in Table 1). The equivalent damping ratio of the uncontrolled structure is about 4.0%, while the equivalent damping ratio of the structure with lateral damping buffer is 5.2%–7.5%, with improvement being 30.0%–87.5%. The lateral damping buffer has control effectiveness on account of the subsequent structural vibration.

Table 1. Equivalent damping ratio (%).

Loading Grades	1	2	3	4	5	6	7	8	9	10
Uncontrolled	4.0	4.0	4.0	4.0	4.0	4.0	4.0	4.0	4.0	4.0
With isolators	5.2	6.2	6.1	6.2	5.4	6.1	6.7	7.5	7.0	6.3
Improvement	30.0	55.0	52.5	55.0	35.0	52.5	67.5	87.5	75.0	57.5

4. Numerical Simulation

As introduced in Section 2, a lateral damping buffer can be regarded as a combination of a buffer and a shock absorber. Meanwhile, the element of the buffer functions in a remarkably short period of time, mainly in the vicinity of the moment of impact. Specifically, the peak value of the acceleration of the controlled structure is reduced greatly compared to the uncontrolled structure. In this limited timespan, the shock absorber has not come into action yet because the increase of the damping coefficient by the collision of the boxes and particle takes time. Then, after impact, the portion of the shock absorber functions step by step and reduces the subsequent vibration of the primary structure gradually. In summary, the two roles of the lateral damping buffer take effect in different periods of time: the buffer portion works in a short time in the vicinity of the impact, while the shock absorber portion works mainly in the process of the structural vibration after impact. Consequently, the effectiveness of the two parts can be considered respectively.

To simulate the whole process of the structural vibration reasonably, the process of the response of the structure is divided into two parts: the maximum acceleration and the root mean square of the subsequent response.

4.1. The Cushion Phase

In this section, the buffer action of the device is the main consideration and the calculation of peak acceleration is the major subject. The structure is simulated as an entirety with infinite rigidity of the beam assumption and the steel ball is simplified to a particle. In addition, the buffer is simulated by a contact spring. The mechanical model is shown in Figure 7. The equations of motion can be established on the basis of the *D'alembert principle*.

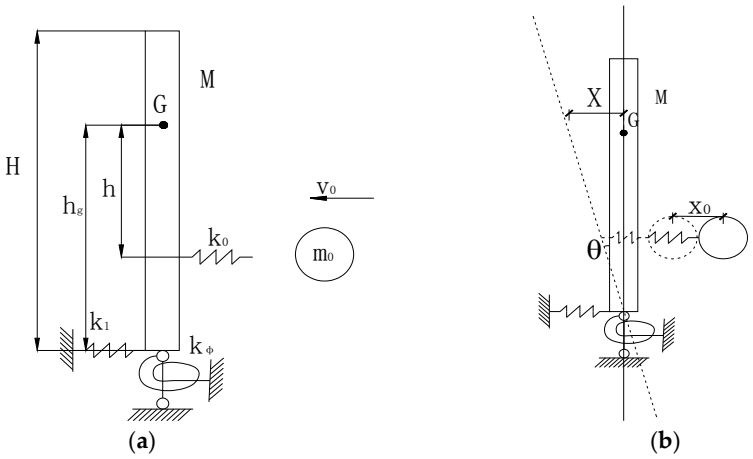

Figure 7. Mechanical model: (**a**) Geometric parameters; (**b**) Motion parameters.

In the system shown in Figure 7, m_0 and M represent the impact ball and the primary structure respectively, k_0, k_1, and k_Φ denote the stiffness of the contact spring, the lateral bracing rigidity and the anti-rotation stiffness of the structure respectively, H, h_g, h stand for the total height of the structure, the height of the center of gravity from the bottom of the structure and the difference of height between the center of gravity and the contact spring respectively, and J means inertia rotation.

In the process of the impact, the displacement of the steel ball m_0 is represented by x_0, the displacement of the primary structure is represented by X, the rotational angle at the bottom of the structure is represented by θ, and the bottom lateral translation of the structure is small enough to be neglected. Meanwhile, the influence of the damping is not considered because the peak value appears at the very beginning of the process of the response and the damping has not come into play to reduce the vibration. The equation of motion is given as:

$$\begin{aligned} m_0\ddot{x}_0 + k_0[x_0 - (x_1 - h\theta)] &= 0 \\ M\ddot{X} + k_0[x_0 - (x_1 - h\theta)] &= 0 \\ J\ddot{\theta} + k_\varphi \varphi + k_0 h[x_0 - (x_1 - h\theta)] &= 0 \end{aligned} \tag{1}$$

The velocities v_0 of the steel ball in different loading grades can be calculated by the theorem of kinetic energy (shown in Table 2). Therefore, the equation of motion can be solved and the simulated peak values of the acceleration response of the structure in different loading grades can be obtained.

Table 2. Impact velocities of the iron ball.

Loading Grades	1	2	3	4	5	6	7	8	9	10
Height (m)	0.05	0.1	0.15	0.2	0.25	0.3	0.35	0.4	0.45	0.5
Velocity (m/s)	0.77	1.08	1.33	1.53	1.71	1.88	2.03	2.17	2.3	2.42

4.2. The energy Dissipation Phase

To study the vibration damping performance of the shock absorber portion, the root mean square response of the subsequent waves is calculated. The structure with the lateral damping buffer is simplified as a 3-DOF model (the primary structure is 2-DOF and the lateral damping buffer is the third DOF), and the equation of motion is established. The waveband where the peak value is located has been obtained in Section 4.1. Therefore, the velocity and the acceleration at the end of the mentioned waveband can be regarded as initial conditions to solve the equation.

The equation of the motion is given as:

$$[K]\{x\} + [C]\{\dot{x}\} + [M]\{\ddot{x}\} = 0 \tag{2}$$

where stiffness matrix $[K] = \begin{bmatrix} k_1 + k_2 + k_3 & -k_2 & -k_3 \\ -k_2 & k_2 & 0 \\ -k_3 & 0 & k_3 \end{bmatrix}$; mass matrix $[M] = \begin{bmatrix} m_1 & 0 & 0 \\ 0 & m_2 & 0 \\ 0 & 0 & m_3 \end{bmatrix}$; damping matrix $[C]$ is determined according to the Rayleigh damping assumption. m_1, m_2, m_3 represent the mass of the first storey and the second storey of the primary structure, as well as the mass of the lateral damping buffer, respectively; k_1, k_2, k_3 represent the stiffness of the first storey and the second storey of the primary structure, as well as the stiffness of the lateral damping buffer, respectively, and $\{x\}$, $\{\dot{x}\}$, $\{\ddot{x}\}$ represent the displacements, velocities and accelerations of both the primary structure and the lateral damping buffer given by the impact.

4.3. Calculation Parameters

In the test, the primary structure with added mass weighs 6.9 kg totally, so $m_1 = m_2 = 3.45$ kg, and the mass of the lateral damping buffer m_3 = 0.33 kg. The first and second order frequencies of the structure are $f_1 = 3.56$ Hz and $f_2 = 14.07$ Hz. The stiffness of the structure is $k_1 = k_2 = 10085$ N/m. Moreover, the stiffness of the buffer is obtained by measurement, $k_3 = 2321.4$ N/m.

The damping matrix $[C]$ is determined according to the Rayleigh damping assumption

$$[C] = \begin{bmatrix} 35.25 & -9.14 & -1.65 \\ -9.14 & 24.46 & 0 \\ -1.65 & 0 & 3.11 \end{bmatrix} \text{N·s·m}^{-1}$$

4.4. Calculation Results

In this paper, the numerical simulation is accomplished. The experimental maximum acceleration and the calculated maximum acceleration are shown in Figure 8. The curves of experimental and calculated acceleration time histories are shown in Figure 9. It can be seen that the calculated values

agree well with the experimental results. Extraordinarily, the calculated peak value shows high degree of fit. Considering the debris flow characteristics of high velocity, strong striking force and severe destruction, the study aimed at peak value of the response is more meaningful.

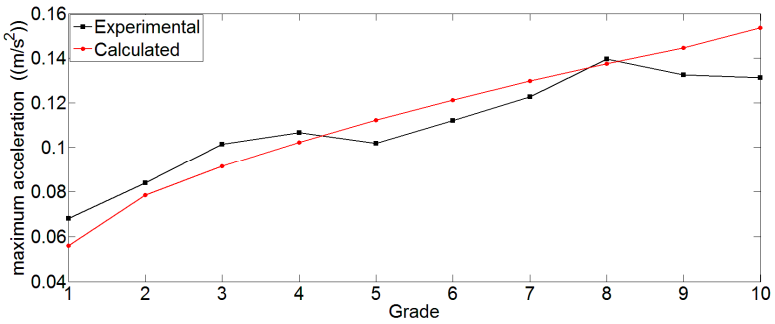

Figure 8. The comparison of the experimental and calculated maximum acceleration.

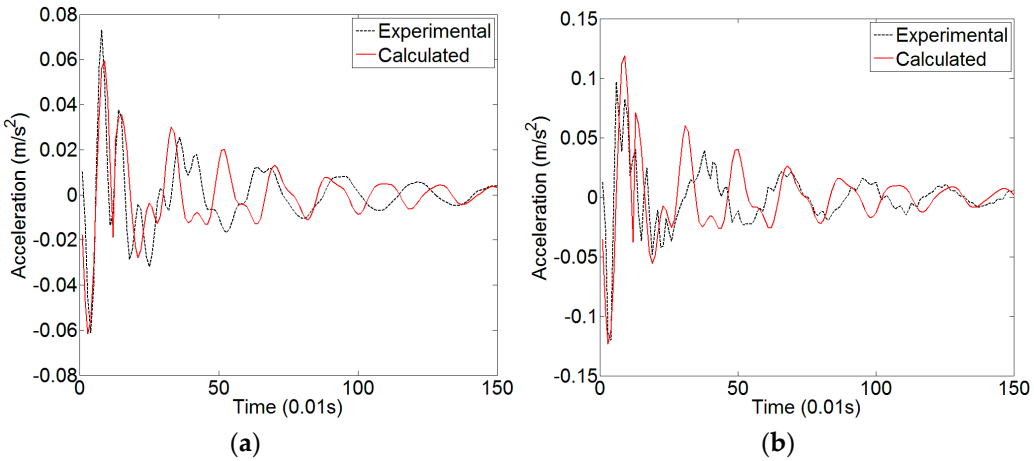

Figure 9. The comparison of the experimental and calculated time history curves: (**a**) Grade 2; (**b**) Grade 8.

4.5. Parametric Study

To study the influence of different parameters and obtain reasonable design of the lateral damping buffer, the effects of its contact stiffness, damping ratio and the mass ratio are discussed.

4.5.1. Contact Stiffness

To study the influence of contact stiffness on the effectiveness of the lateral damping buffer, the response of the primary structure can be calculated by the methods above with different contact stiffness. The initial velocity is taken as the velocity in grade 5, and the contact stiffness ranges from 1000 N/m to 3000 N/m. Then, the peak values of the structural response (as shown in Figure 10) are calculated by the methods mentioned in Section 4.1.

From Figure 10, it can be seen that the maximum acceleration increases with the enlargement of the contact stiffness. In other words, the decrease of the contact stiffness can improve the reduction performance, but there is a deformation limit for springs in reality. Therefore, although the relative "soft" spring is preferred, the choice of contact stiffness will also be constrained by practical considerations. That is, the relative "soft" spring is preferred according to the parametric study. However, the stiffness of the spring cannot be infinitely small. There is a restriction, which is the limit of spring deformation. At the very least, it should be ensured that the spring can operate normally under the impact load of debris flow, and this is related to site investigation of the designed target area.

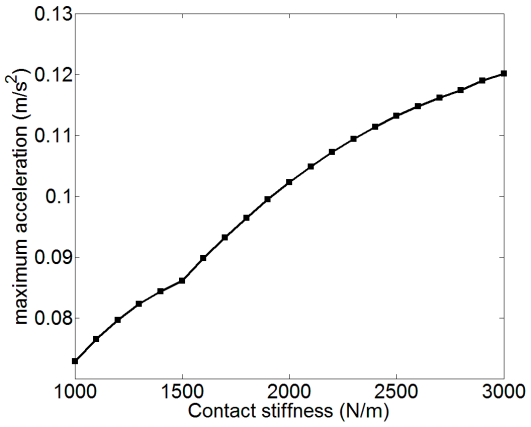

Figure 10. The influence of the contact stiffness.

4.5.2. Damping Ratio

To study the influence of the damping ratio, the response of the primary structure can be calculated by methods illustrated in Section 4.2 with different damping ratios. The initial velocity and initial acceleration are taken as the velocity and acceleration in grade 5, and the damping ratio is taken as ξ = 0.04, 0.05, 0.06, 0.07, 0.08, and 0.09. Then, the root mean square accelerations (as shown in Figure 11) are calculated by the methods in Section 4.2.

From Figure 11, it can be seen that the root mean square accelerations decrease with the enlargement of the damping ratios. In other words, the increase of the damping ratio can improve the reduction performance. Hence, by optimizing the parameters of the boxes and the particles, the structural damping can be increased, thereby reducing the subsequent structural vibration.

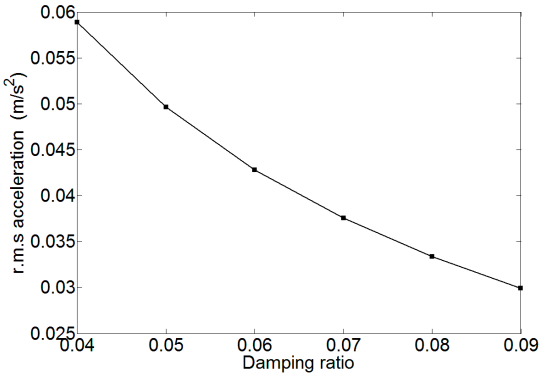

Figure 11. The influence of the damping ratio.

4.5.3. Mass Ratio

To study the influence of the mass ratio (the ratio of total auxiliary mass, including the boards, springs, particles and boxes, to the mass of test model), we can calculate the response of the structure by the methods in Sections 4.1 and 4.2 with different mass ratios. The mass ratio is different from the previous two parameters in that it affects both the structural response in two phases. Therefore, the analysis of this parameter can be considered from the two aspects of peak acceleration and root mean square acceleration, respectively. The initial velocity and initial acceleration are taken as the velocity and acceleration in grade 5, and the mass ratio ranges from 1.0% to 4.0%. Then, the response reduction effects of the peak acceleration and the root mean square acceleration (as shown in Figure 12) are calculated by the methods in Sections 4.1 and 4.2.

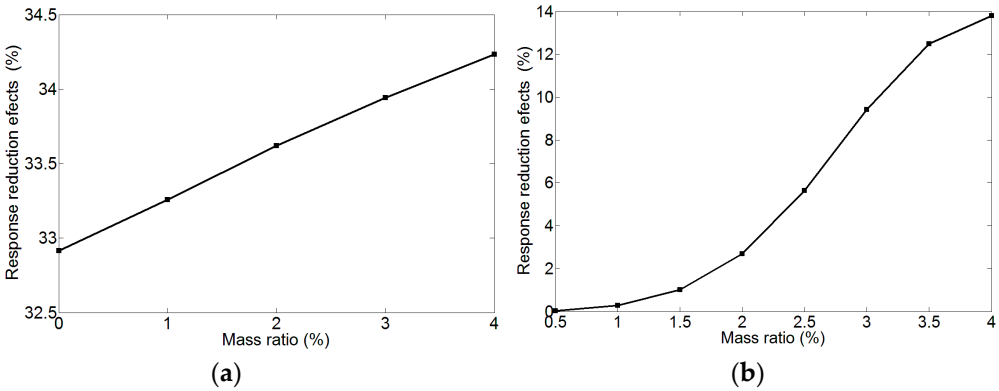

Figure 12. The influence of the mass ratio: (**a**) Maximum acceleration; (**b**) r.m.s acceleration.

From Figure 12a, it can be seen that with the increase of mass ratio, the decrease rate of the peak response of the structure increases monotonously, but the increase range is small, indicating that the increase of the mass ratio has a certain effect on reducing the peak response of the structure, but the effect is not prominent. In Figure 12b, the variation of the root mean square response reduction rate is the same as in Figure 12a in general. However, the rate of increase of the root mean square reduction rate is obviously faster when the mass ratio is changed from 2.0% to 3.5%. Moreover, the influence of the mass ratio on the root mean square response reduction is obviously greater than that on the peak response. The design of the device can be considered in terms of its impact on both of the root mean square response and the peak response. However, in practice, it is clear that the peak response of the structure is more meaningful considering the characteristics of the debris flow load.

5. Design Procedure

According to the mechanisms and parametric study of the lateral damping buffer, the design process of such a buffer in resisting the debris flows is proposed, as shown in Figure 13.

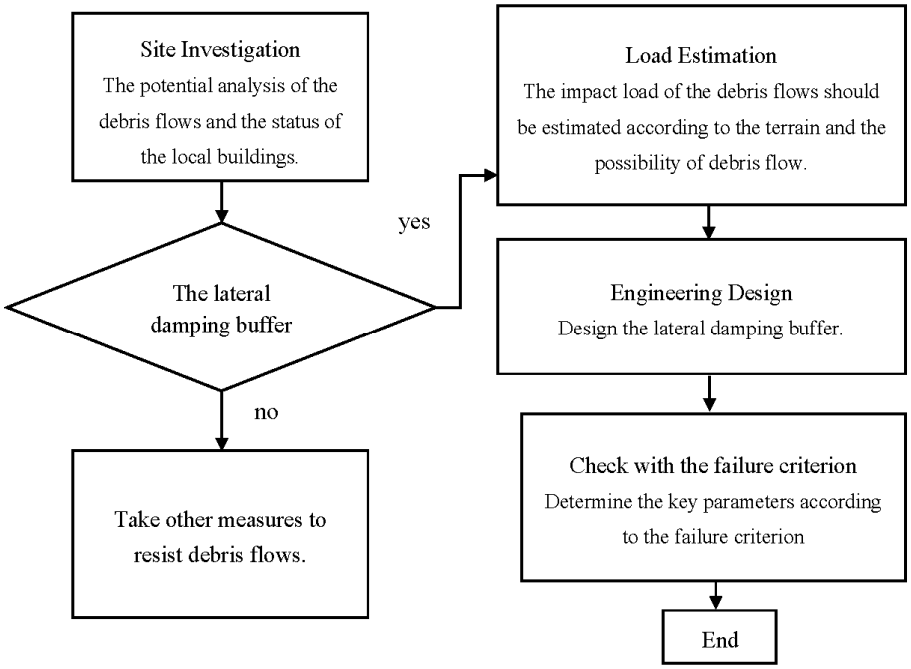

Figure 13. The design process of the lateral damping buffer in resisting debris flows.

The buffer is mainly made of boards, springs, particles and boxes. The specific steps to determine the necessary parameters for engineering design are described below.

(1) The size of the boards should be determined based on the specific engineering information of the target area, especially the statistical characterizations of the vulnerable debris flows. The length of the boards should be equal to the length of target buildings facing debris flows, and the height should be determined by the impact height of debris flows. For example, the height of the board can be twice of the height of the impact height;
(2) The stiffness of the springs should be determined by numerical simulation and the actual circumstance, considering the debris flow load, spring deformation limit and disaster reduction effect synthetically. Generally, a relative "soft" spring is preferred according to the parametric study. However, its stiffness is also constrained by the workability under the impact load of debris flows;
(3) The mass of particles and boxes should be determined by the mass ratio, which is the mass of particles and boxes to the mass of the primary structure. For the determination of sizes, refer to the previous study on filling ratio in particle damping technology [36,37].

In addition, the failure criterion is related to the regulations in the code. For example, in the "Code for Seismic Design of Buildings" [38] in China, the maximum inter-story drift under major earthquake is regulated as 1/50, and this value can be used to be a kind of failure criterion.

6. Conclusions

In this paper, we propose and study a new type of device, named a lateral damping buffer, to reduce the vulnerability of building structures to debris flows. The lateral damping buffer can be regarded as a combination of a buffer and a shock absorber, which can reduce the maximum acceleration response and the subsequent vibration respectively. To examine the effectiveness of the lateral damping buffer, an impact test of the lateral damping buffer attached to a two-degree-of-freedom structure under the simulated debris flows load is completed. After the test, a corresponding numerical simulation is performed to validate its rationality. Then, a following parametric study is performed to optimize the lateral damping buffer. Finally, an engineering design procedure is put forward.

The impact test shows that the lateral damping buffer has good effectiveness in reducing both the maximum acceleration response and the subsequent vibration. Particularly for the tenth loading grade, the maximum acceleration response can be reduced by nearly half and the root mean square acceleration can be reduced by over 30%. In addition, the simulated values fit well with the experimental results. Moreover, the effectiveness of the lateral damping buffer increases with the increase in the loading grade. This characteristic is beneficial to the application in practical engineering.

The lateral damping buffer can also reduce the subsequent vibration of the primary structure by energy dissipation. However, considering the characteristics of the debris flows, the attachment of the cushion devices at the impact point is more effective.

Acknowledgments: Financial support from the National Key Technology R&D Program through grant 2014BAL05B01 is highly appreciated.

Author Contributions: Zheng Lu proposed the new device, conceived the experiments and wrote the paper; Yuling Yang performed the experiments and analyzed the data; Xilin Lu provided valuable discussions and revised the paper; Chengqing Liu proposed the new device, conceived and designed the experiments and revised the paper.

Conflicts of Interest: The authors declare no conflict of interest.

References

1. Osti, R.; Egashira, S. Method to improve the mitigative effectiveness of a series of check dams against debris flows. *Hydrol. Processes* **2008**, *22*, 4986–4996. [CrossRef]

2. Hu, K.H.; Zhang, J.Q. Characteristics of damage to buildings by debris flows on 7 August 2010 in Zhouqu, Western China. *Nat. Hazards Earth Syst. Sci.* **2012**, *12*, 2209–2217. [CrossRef]
3. Zanuttigh, B.; Lamberti, A. Experimental analysis of the impact of dry avalanches on structures and implications for debris flows. *J. Hydraul. Res.* **2006**, *44*, 522–534. [CrossRef]
4. Chen, J.G.; Chen, X.Q.; Li, Y.; Wang, F. An experimental study of dilute debris flow characteristics in a drainage channel with an energy dissipation structure. *Eng. Geol.* **2015**, *193*, 224–230. [CrossRef]
5. Chen, X.Q.; Cui, P.; You, Y.; Chen, J.G.; Li, D.G. Engineering measures for debris flow hazard mitigation in the Wenchuan earthquake area. *Eng. Geol.* **2014**, *194*, 73–85. [CrossRef]
6. You, Y.; Pan, H.L.; Liu, J.F.; Ou, G.Q. The optimal cross-section design of the "Trapezoid-V" shaped drainage channel of viscous debris flow. *J. Mt. Sci.* **2011**, *8*, 103–107. [CrossRef]
7. Armanini, A.; Larcher, M. Rational criterion for designing opening of slit-check dam. *J. Hydraul. Eng.* **2001**, *127*, 94–104. [CrossRef]
8. Chanson, H. Sabo check dams-mountain protection systems in Japan. *Int. J. River Basin Manag.* **2004**, *2*, 301–307. [CrossRef]
9. Hassanli, A.M.; Nameghi, A.E.; Beecham, S. Evaluation of the effect of porous check dam location on fine sediment retention (a case study). *Environ. Monit. Assess.* **2009**, *152*, 319–326. [CrossRef] [PubMed]
10. Canelli, L.; Ferrero, A.M.; Migliazza, M.; Segalini, A. Debris flow risk mitigation by the means of rigid and flexible barriers-experimental tests and impact analysis. *Nat. Hazards Earth Syst. Sci.* **2012**, *12*, 1693–1699. [CrossRef]
11. Navratil, O.; Liébault, F.; Bellot, H.; Travaglini, E.; Theule, J.; Chambon, G.; Laigle, D. High-frequency monitoring of debris-flow propagation along the Réal Torrent, Southern French Prealps. *Geomorphology* **2013**, *201*, 157–171. [CrossRef]
12. Okano, K.; Suwab, H.; Kanno, T. Characterization of debris flows by rainstorm condition at a torrent on the Mount Yakedake volcano, Japan. *Geomorphology* **2012**, *136*, 88–94. [CrossRef]
13. Chengdu Institute of Mountain Hazards and Environment, Chinese Academy of Sciences and Ministry of Water Resources. *Debris Flows in China*, 1st ed.The Commercial Press: Beijing, China, 2000. (In Chinese)
14. Yao, J.T.P. Concept of structural control. *J. Struct. Div. ASCE* **1972**, *98*, 1567–1574.
15. Lu, Z.; Lu, X.L.; Lu, W.S.; Masri, S.F. Shaking table test of the effects of multi-unit particle dampers attached to an MDOF system under earthquake excitation. *Earthq. Eng. Struct. Dyn.* **2012**, *41*, 987–1000. [CrossRef]
16. Zhou, Y.; Zhang, C.Q.; Lu, X.L. Seismic performance of a damping outrigger system for tall buildings. *Struct. Control. Health Monit.* **2016**, *24*. [CrossRef]
17. Lu, Z.; Lu, X.L.; Jiang, H.J.; Masri, S.F. Discrete element method simulation and experimental validation of particle damper system. *Eng. Comput.* **2014**, *31*, 810–823. [CrossRef]
18. Zhang, P.; Song, G.B.; Lin, Y. Seismic Control of Power Transmission Tower Using Pounding TMD. *J. Eng. Mech.* **2013**, *139*, 1395–1406. [CrossRef]
19. Lu, Z.; Chen, X.Y.; Lu, X.L.; Yang, Z. Shaking table test and numerical simulation of an RC frame-core tube structure for earthquake-induced collapse. *Earthq. Eng. Struct. Dyn.* **2016**, *45*, 1537–1556. [CrossRef]
20. Poussot-Vassal, C.; Spelta, C.; Sename, O.; Savaresi, S.M.; Dugard, L. Survey and performance evaluation on some automotive semi-active suspension control methods: A comparative study on a single-corner mode. *Annu. Rev. Control* **2012**, *36*, 148–160. [CrossRef]
21. Poussot-Vassal, C.; Sename, O.; Dugard, L.; Gaspar, P.; Szabo, Z.; Bokor, J. A new semi-active suspension control strategy through LPV technique. *Control Eng. Pract.* **2008**, *16*, 1519–1534. [CrossRef]
22. Lozoya-Santos, J.D.J.; Hernandez-Alcantara, D.; Morales-Menendez, R.; Ramirez-Mendoza, R.A. Modeling of dampers guided by their characteristic diagrams. *Rev. Iberoam. Autom. Inf. Ind.* **2015**, *12*, 282–291. [CrossRef]
23. Lozoya-Santos, J.D.J.; Morales-Menendez, R.; Ramirez-Mendoza, R.A. Evaluation of on-off semi-active vehicle suspension systems by using the hardware-in-the-loop approach and the software-in-the-loop approach. *Proc. Inst. Mech. Eng. D J. Autom. Eng.* **2015**, *229*, 52–69. [CrossRef]
24. Poussot-Vassal, C.; Sename, O.; Dugard, L.; Gaspar, P.; Szabo, Z.; Bokor, J. Attitude and handling improvements through gain-scheduled suspensions and brakes control. *Control Eng. Pract.* **2011**, *19*, 252–263. [CrossRef]
25. Li, H.N.; Zhang, P.; Song, G.B.; Li, L.; Patil, D.; Mo, Y.L. Robustness study of the pounding tuned mass damper for vibration control of subsea jumpers. *Smart Mater. Struct.* **2015**, *24*, 1–12. [CrossRef]

26. Zhang, P.; Li, L.; Patil, D.; Singla, M.; Li, H.N.; Mo, Y.L.; Song, G.B. Parametric study of pounding tuned mass damper for subsea jumpers. *Smart Mater. Struct.* **2016**, *25*, 1–7. [CrossRef]
27. Lu, Z.; Wang, D.C.; Masri, S.F.; Lu, X.L. An experimental study of vibration control of wind-excited high-rise buildings using particle tuned mass dampers. *Smart Struct. Syst.* **2016**, *25*, 1–7. [CrossRef]
28. Lu, Z.; Chen, X.Y.; Zhang, D.C.; Dai, K.S.; Masri, S.F.; Lu, X.L. Experimental and analytical study on the performance of particle tuned mass dampers under seismic excitation. *Earthq. Eng. Struct. D* **2016**. [CrossRef]
29. Dai, K.S.; Wang, J.Z.; Mao, R.F.; Lu, Z.; Chen, S.E. Experimental investigation on dynamic characterization and seismic control performance of a TLPD system. *Struct. Des. Tall Spec. Build.* **2016**. [CrossRef]
30. Gong, S.M.; Zhou, Y.; Zhang, C.Q.; Lu, X.L. Experimental study and numerical simulation on a new type of viscoelastic damper with strong nonlinear characteristics. *Struct. Control Health* **2016**. [CrossRef]
31. Zhang, Y.; Wei, F.Q.; Wang, Q. Dynamic response of buildings struck by debris flows. Debris-Flow Hazards Mitigation: Mechanics, Prediction, and Assessment. In Proceedings of the 4th International Conference on Debris-Flow Hazards Mitigation—Mechanics, Prediction, and Assessment, Chengdu, China, 10–13 September 2007.
32. Clough, R.W.; Penzien, J. Analysis of free vibration. In *Dynamics of Structures*, 3rd ed.; Computers & Structures, Inc.: Berkeley, CA, USA, 2003.
33. Zhang, Y.; Wei, F.Q.; Jia, S.W.; Liu, B. Experimental research of unreinforced masonry wall under dynamic impact of debris flow. *J. Mt. Sci.* **2006**, *24*, 340–345. (In Chinese)
34. Kozo, O.; Hiroki, T.; Hendro, S. Shock-absorbing capability of lightweight concrete utilizing volcanic pumice aggregate. *Constr. Build. Mater.* **2015**, *83*, 261–274.
35. Japan Society of Civil Engineers. *Practical Methods for Impact Test and Analysis*; Maruzen: Tokyo, Japan, 2004. (In Japanese)
36. Lu, Z.; Masri, S.F.; Lu, X.L. Parametric studies of the performance of particle dampers under harmonic excitation. *Struct. Control Health* **2011**, *18*, 79–98. [CrossRef]
37. Lu, Z.; Wang, D.C.; Zhou, Y. Experimental parametric study on wind-induced vibration control of particle tuned mass damper on a benchmark high-rise building. *Struct. Des. Tall Spec. Build.* **2017**. [CrossRef]
38. PRC Ministry of Housing and Urban-Rural Development; General Administration of Quality Supervision, Inspection and Quarantine of the People's Republic of China. *Code for Seismic Design of Buildings (GB50011-2010)*; China Architecture & Building Press: Beijing, China, 2010. (In Chinese)